THE JOURNAL OF PHYSICAL CHEMISTRY C LETTERS

2009, *113,* 6315–6319
Published on Web 03/31/2009

LETTERS

Enhancement and Confinement Analysis of The Electromagnetic Fields Inside Hot Spots

Eduardo M. Perassi,[†] Luis R. Canali,[‡] and Eduardo A. Coronado*[,†]

INFIQC, CLCM, Dpto. de Fisicoquímica, Facultad de Ciencias Químicas, Universidad Nacional de Córdoba, Córdoba 5000, Argentina, and CIII, Universidad Tecnológica Nacional, Facultad Regional Córdoba, Córdoba 5000, Argentina

Received: December 19, 2008; Revised Manuscript Received: March 20, 2009

A novel and easy approach to implement is developed to analyze the degree of convergence, confinement, and enhancement (Γ) of calculated electromagnetic fields generated in plasmonic nanoparticles (NPs) of arbitrary shape. The approach is based on computing the variation of the volume trapped (V_T) between a constant Γ surface around a metal NP and the nanoparticle surface boundary as a function of the enhancement itself. This method is a new and a more practically relevant approach to test the convergence than measures traditionally employed. For the test cases outlined here, the converged V_T vs Γ curve could be fitted very accurately to a triple exponential expression which makes it convenient to determine the mean field enhancement within a trapped volume outside the NP, as well as the degree of localization and spreading of the hot spots (HSs) in 3D space. The technique introduced here should aid the understanding and a rational design of plasmonic devices based on metal NPs, where the near field plays a major role, such as in plasmon enhanced spectroscopies and plasmon imaging.

Noble metal nanoparticles (NPs) exhibit a variety of optical phenomena related to the size and shape dependent surface plasmon resonances (SPR) that can be excited by electromagnetic fields.[1−3] Such optical phenomena are able to produce large scattering cross sections at specific wavelengths as well as strongly confined and enhanced electromagnetic fields in spatial regions usually called hot spots (HSs).[4−6] HSs are critically important to all plasmon enhanced spectroscopies such as surface-enhanced raman scattering (SERS),[5,7−11]tip-enhanced raman spectroscopy (TERS),[12−14] metal-enhanced fluorescence (MEF),[2,15,16] and even single-molecule spectroscopy (SM-SERS),[17,18] which have opened the way to a variety of applications such as biosensors,[9,19,20] plasmon nanolithography,[21] and probes for scanning near optic microscopy (SNOM),[4,22] among others.

It is therefore of great importance to be able to accurately determine the electromagnetic field enhancement as well as its degree of localization inside a HS, both from basic science and for applications in plasmonic devices. For example, an accurate determination of the electromagnetic field enhancement is very important to evaluate the relative contribution of the chemical and electromagnetic mechanism proposed for SERS or to evaluate the distance dependence of SERS, TERS, and MEF around a nanostructure.[23,24] SM-SERS is perhaps the application where the above-mentioned issues are particularly relevant since recent experiments have demonstrated that the electromagnetic mechanism is all that is required to explain the observed single molecule sensitivity.[25]

The electromagnetic field enhancement (Γ), in a given point of space, will be defined as $\Gamma = \mathbf{E}\cdot\mathbf{E}^*/\mathbf{E_0}\cdot\mathbf{E_0^*}$, where $\mathbf{E}$ is the complex electromagnetic field at this point and $\mathbf{E_0}$ is the incident field. In order to compute the electromagnetic field enhancement inside a HS there are analytical solutions for particles with simple shapes, like spheres and spheroids, while for other shapes a number of numerical methods have been developed such as the finite difference time-domain, (FTDT),[9,26] the discrete-dipole approximation (DDA), the multiple multi-pole technique (MMT),[27] and the T-MATRIX method, to name some of the most popular ones.[28]

Accounting for the high local variation of the electromagnetic field at a HS is a problem that any electrodynamic calculation has to deal with, and it is an issue which is directly related to the convergence of the method with respect to the multipole order used in the expansions in some analytical methods or to the grid size parameter in the numerical approaches.[29]

In this work, we choose the DDA method because this is a particularly powerful method for isolated NPs or small aggregates in a complex surrounding environment and can be applied for arbitrary shaped NPs and arrays. In this method the object of interest is represented as a cubic array of N polarizable elements.[3,30−33] The optical response of this array is determined by solving in a self-consistent way the induced dipole moments in each element. The output of this procedure can be used to determine far field optical properties (scattering and extinction cross sections), as well as near field optical properties, such as

* To whom correspondence should be addressed. E-mail: coronado@mail.fcq.unc.edu.ar.
[†] INFIQC.
[‡] CIII.

10.1021/jp811256e CCC: $40.75

the electromagnetic field close to the NPs. The grid spacing (d) of this cubic array is a key parameter for a high quality simulation of the far field and near field optical properties.

Although the convergence criteria is almost evident for the computation of the far field optical properties, i.e., when any significant variation of the extinction spectra is produced upon changing the grid spacing, the criteria of convergence for the near field is less obvious. One approach commonly used is to vary the grid spacing and compute the electric filed enhancement versus some distance for a direction along the polarization vector.[34] Although this criteria could be very useful for some applications, it has some degree of arbitrariness in choosing the plane as well as the direction along which the field enhancement is computed, specially for particles of arbitrary shape.

Another important aspect that needs to be considered is not only the value of the field enhancement but also a measure definition of the degree of localization of the enhanced fields around the NP, a parameter of fundamental importance for many plasmonic applications such as those mentioned above.

In this letter, we introduce the concept of variation of the trapped volume (VTV) which will allow us to characterize the enhancement of the electromagnetic field and its localization inside a HS as well as to give a convergence criteria for the electrodynamics method used.

Here we will be focused on HSs around single metal NPs so that the trapped volume (V_T) will be defined as the volume enclosed between a constant Γ surface around a metal NP and the NP surface boundary. A plot of V_T vs Γ for different grid spacing results in a series of curves that will be termed as VTV curves. If convergence has been reached the trapped volume for a value of the enhancement should be invariant upon changing the grid size.

In order to show the capabilities of the VTV approach, we have computed V_T vs Γ for HSs generated around silver NPs in vacuum for three different shapes: prolate spheroid, cylinder, and triangular prism. In all of the calculations, we have used the dielectric function tabulated by Palik.[35] Surface scattering corrections or quantum size effects were not taken into account since the main purpose of this work is to test the VTV approach. Including such a correction on the dielectric constant should produce smaller values of Γ, specially for the prolate spheroid NP, but it does not have any implications on the results and conclusions of this work. The computation of Γ and V_T were performed using a customized version of DDSCAT 6.1 program (see the Supporting Information for more details).

Figure 1a shows the VTV curves for a prolate spheroid with an aspect ratio ar = 2 (ar = major axis/minor axis) when illuminated at λ = 432 nm with polarization along the major axis, having the dimensions indicated in the inset of this figure. In order to compute V_T for different grid spacing we have taken only one of the HS generated in one end of the NP. There is certainly a great variation of the VTV curves varying the grid spacing, but after some critical value of $d \approx 0.1654$ nm, all the VTV curves become indistinguishable. At this point we can ensure that this curve represents the most reliable variation of V_T with Γ. For comparison, it should be noted that the extinction spectra for this NP (not shown) is fully converged using $d \approx$ 0.5 nm, which indicates a more demanding computational effort needed to calculate near field optical properties accurately.

A "tomography" of the converged enhancement field distribution is depicted in Figure 1b for the planes indicated in the inset of Figure 1a. These planes were chosen taking into account the symmetry of the Γ distribution with respect to planes C and F. The maximum field enhancement is achieved, as expected for

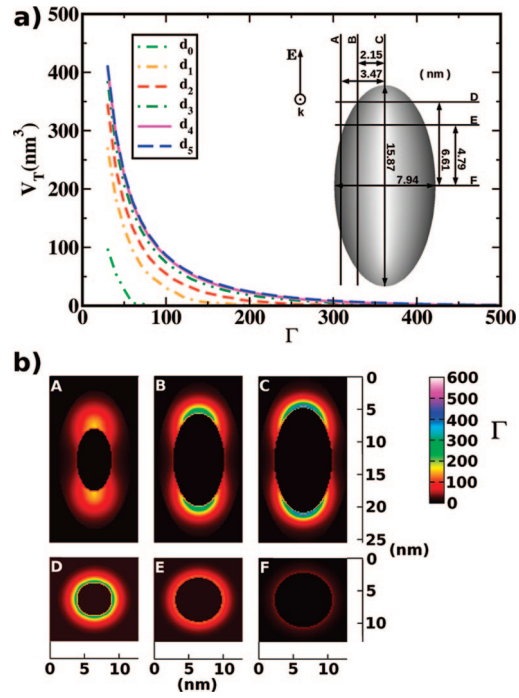

Figure 1. (a) VTV curves for a prolate Ag NP with aspect ratio ar = 2, for different values of grid size parameter (d): d_0 = 0.9922 nm, d_1 = 0.4967 nm, d_2 = 0.3310 nm, d_3 = 0.1985 nm, d_4 = 0.1654 nm, d_5 = 0.1417 nm. The incident electromagnetic field wavelength is λ = 432 nm, and the polarization is along the major axis. The inset outlines the NP dimensions as well as the planes chosen to plot the electric field enhancement (Γ) distribution. (b) Images of the electric field enhancement for each of the planes outlined in the inset of panel a.

a dipole SPR, at both ends of the major axis along the polarization direction. As it can be appreciated from these images, the Γ values are larger for the plane closer to the nanoparticle tip (plane D), reaching the maximum values on plane C and the negligible ones on plane F.

We will now consider as a second example a silver nanocylinder (whose dimensions are indicated in the inset of Figure 2a), illuminated with polarization along the major axis at λ = 537 nm. It should be noted that the trapped volume considered here corresponds to either one equivalent HS generated at either end of this NP. Computation of the VTV curves for different grid spacing indicates that for $d \approx 0.3627$ nm convergence has been achieved as shown in Figure 2a. The corresponding tomography of the electromagnetic field enhancement is depicted in Figure 2b for some representative planes, perpendicular (planes D, E, and F) and parallel (planes A, B, and C) to the NP major axis (indicated in the inset of Figure 2a). At variance with the silver spheroid, the highest enhancement is found around the perimeter of the circle surrounding both ends of the major axis.

As a final example, we will examine a silver triangular nanoprism with equal edge lengths, illuminated on a direction perpendicular to the triangular cross section, with polarization along the height of the triangular face. The actual dimensions and geometry of this NP as well as the planes chosen to plot the enhancement distribution are indicated in the inset of Figure 3a. In this case, there are six regions of maximum field enhancement located at each of the six vertexes of the nanoprism. From the three HSs on each face of the triangular prism (which are a mirror image of the HS's on the other triangular face), there is one whose enhancement is on average greater than the other two as shown in Figure 3b. For the computation of the VTV curves we have chosen the volume

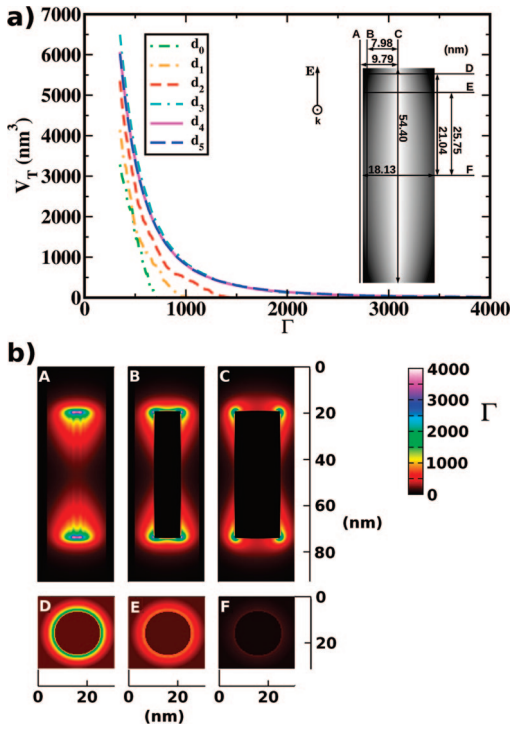

Figure 2. (a) VTV curves for a cylinder Ag NP with aspect ratio ar = 3, for different values of grid size parameter (d): $d_0 = 2.2459$ nm, $d_1 = 1.5192$ nm, $d_2 = 1.1229$ nm, $d_3 = 0.5044$ nm, $d_4 = 0.3627$ nm, $d_5 = 0.3028$ nm. The incident electromagnetic field wavelength is $\lambda = 573$ nm and the polarization is along the major axis. The inset outlines the NP dimensions as well as the planes chosen to plot the electric field enhancement (Γ) distribution. (b) Images of the electric field enhancement for each of the planes outlined in the inset of panel a.

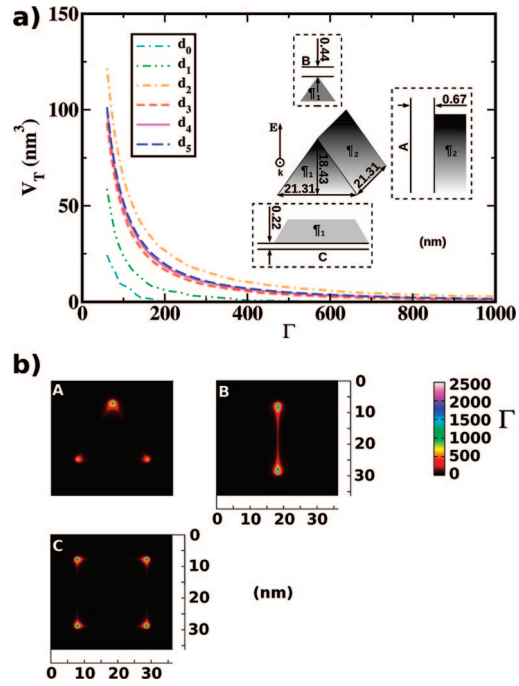

Figure 3. (a) VTV curves for a triangular nanoprism with equal edge lengths Ag NP, for different values of grid size parameter (d): $d_0 = 0.6656$ nm, $d_1 = 0.4439$ nm, $d_2 = 0.2664$ nm, $d_3 = 0.2422$ nm, $d_4 = 0.2220$ nm, $d_5 = 0.1776$ nm. The incident electromagnetic field wavelength is $\lambda = 465$ nm, the propagation direction is perpendicular to the triangular cross section while the polarization is along the height of the triangular face. The inset outlines the NP dimensions as well as the planes chosen to plot the electric field enhancement (Γ) distribution. (b) Images of the electric field enhancement for each of the planes outlined in the inset of panel a.

encompassed by one of the hottest spot. The VTV curves obtained for different grid spacing are shown in Figure 3a, indicating that convergence is reached for $d = 0.222$ nm. A 3D slicing of the electromagnetic field enhancement for three relevant planes at very small distances from the NP (planes *A*, *B*, and *C*) is shown in Figure 3b, where it can be appreciated the description outlined above concerning the equivalence of the HSs. For the enhancement distribution on plane *B*, we note two equivalent HSs that spread along the NP edge. The analysis of the distribution of Γ through plane *C* shows the four less intense HS's mentioned above, but at variance with the other two (more intense HSs), they are localized around the corners and do not spread around the edges.

So far, we have shown the capabilities of the VTV approach to analyze the convergence of the electrodynamics simulations and the importance of performing a detailed 3D mapping of the electromagnetic field enhancement on different planes around HSs. As it has been pointed out, two relevant quantities in most of the plasmonic applications mentioned above are the maximum field enhancement achievable and the degree of confinement of Γ for a given HS. The first one is of utmost importance, since many numerical electrodynamic methods often fail to asses it, as there are serious numerical problems to calculate the enhancement in regions very close to the NP surface, which corresponds here to a region within a very small trapped volume. The second quantity plays a central role, for example, in estimating the distance dependence of the sensing capabilities within a given HS or the resolution achievable in plasmonic imaging and lithography. Our approach to give an answer to these questions consists in finding a convenient mathematical expression ($V_T(\Gamma)$) for each of the converged VTV curves obtained for the different NPs.

According to the behavior of the converged VTV curves for the three case studies analyzed, and using elementary physical arguments, $V_T(\Gamma)$ should fulfill the following conditions:

(a) it should be positive and strictly decreasing
(b) it should go to zero for a finite value of Γ ($\Gamma_{V_T=0}$)
(c) it should not be defined or should not have any physical sense for $\Gamma > \Gamma_{V_T=0}$

We found that the following expression:

$$V_T(\Gamma) = (\Gamma_{V_T=0} - \Gamma)\sum_{i=0}^{2} A_i e^{-\Gamma/k_i} \quad (1)$$

satisfies the requirements mentioned above and also is able to describe quite accurately the converged variation of V_T with Γ for the three case studies considered in this work. The excellent agreement of fitting the converged DDA calculations with eq 1 is evidenced by the small root-mean-square (rms) deviation values and the excellent correlation coefficients for each optimization as shown in Table 1, along with the corresponding fitting parameters.

Let us now shed some light into the first question pointed out above, i.e., the maximum Γ produced in a given HS, by analyzing eq 1 for each specific case considered in this letter. For $V_T = 0$ eq 1 should give the maximum enhancement when $\Gamma = \Gamma_{V_T=0}$, but this situation corresponds to the unphysical case of an infinitesimally small object. A realistic situation should be to consider the finite volume of a small object suitable to be coupled to the evanescent field of a HS, such as a molecule. For example, let us regard a typical small volume of 0.125 nm^3 which could correpond to a dye molecule such as rhodamine B. Now, it is straightforward, using eq 1, to estimate the

TABLE 1: Parameters of eq 1 for Each Shape Analyzed in This Work

parameters	spheroid	cylinder	prism
$\Gamma_{V_T=0}$	2612	37266	16491
A_0 (nm^3)	0.517	0.649	0.023
k_0	10.7	117.5	26.5
A_1 (nm^3)	0.191	0.370	0.0056
k_1	30.5	268.4	87.1
A_2 (nm^3)	0.0754	0.0494	0.00093
k_2	94.2	761.6	401.5
rms percent error	0.09	1.0	0.02
correlation coefficient	0.999	0.999	0.999

TABLE 2: Field Enhancement ($\Gamma_{V_T=0.125\text{nm}^3}$), average field enhancement ($\bar{\Gamma}_{V_T=0.125\text{nm}^3}$) for $V_T = 0.125$ nm^3 and the Degree of Localization of HSs (Λ) for the Different NPs Shapes Considered in This Work

geometry	$\Gamma_{V_T=0.125\text{nm}^3}$	$\bar{\Gamma}_{V_T=0.125\text{nm}^3}$	Λ (nm^3)
spheroid	666	760	1909
prism	1882	2283	472
cylinder	7146	7907	39557

minimum electromagnetic field enhancement enclosed by this volume for each HS on each NP shape analyzed, as tabulated in Table 2.

From these values, the HS generated around the cylinder NP is able to produce the greatest enhancement followed by the prism and the spheroid. As is evident, this minimum enhancement calculated corresponds to the ideal situation in which the small object (for example the molecule under consideration) can be exactly located within the shape of the volume trapped for each case. In general the shape of V_T does not exactly match the shape of the object under consideration, and no matter how small the object volume would be, it will experience a strong gradient of electromagnetic field enhancement.

As there is a gradient of field enhancement (as V_T decreases the magnitude of Γ increases), it is convenient to define the average enhancement inside a given V_T:

$$\bar{\Gamma} = \Gamma_{\min} + \frac{1}{V_T(\Gamma_{\min})}\int_{\Gamma_{\min}}^{\Gamma_{V_T=0}} V_T(\Gamma)\, d\Gamma \qquad (2)$$

where $\Gamma_{\min}$ is the enhancement for the V_T under consideration. It can easily be shown inserting eq 1 into eq 2 that if the following condition is fulfilled:

$$\Gamma_{\min} \ll \Gamma_{V_T=0} - k_j \qquad \text{with} \quad k_j > k_i \wedge j \neq i \qquad (3)$$

where k_j is the largest coefficient k_i in eq 1, then the mean field enhancement is almost exactly given by the expression:

$$\bar{\Gamma} \approx \Gamma_{\min} + k_j \qquad (4)$$

The above approximation (eq 4) can be used to calculate $\bar{\Gamma}$ inside a $V_T = 0.125$ nm^3 for the three cases analyzed as the condition given by eq 3 is satisfied. These values, shown in Table 2, are slighter larger than $\Gamma_{\min}$.

As a rigorous test on the accuracy of the present VTV approach, we have compared our Γ values with exact electrodynamic calculations performed by Calandera et al.[36] for a prolate gold spheroid with ar = 3 and major axis 63.3 nm illuminated at $\lambda = 633$ nm. The maximum enhancement computed by these authors corresponds to a value very close to the NP surface, so that in order to make the comparison we take the volume of a gold atom ($V_T = 0.0125$ nm^3) and compute the enhancement. We obtained a value of $\sqrt{\Gamma} = 42$, which is in excellent agreement with the exact result $\sqrt{\Gamma} = 47$. (See the Supporting Information for details.)

Let us finally consider the problem of quantifying the degree of localization and spreading of HSs. In order to give an answer to this issue we found it convenient to define a HS as the region of space where the enhancement is greater than one. Using this definition it is straightforward taking $\Gamma = 1$ in eq 1 to obtain the trapped volume that encloses enhancements greater than one. This trapped volume, hereinafter denoted as Λ, constitutes a very useful measure of the degree of localization of each HS, i.e. the smaller Λ, the more confined within the HS will the enhancement be. For the three HSs analyzed in this work the degree of confinement increases in the following order: cylinder < spheroid < prism (see Table 2). This feature, although evident by direct inspection of Figures 1b, 2b, and 3b, can now precisely be quantified for particles of arbitrary shape. Note also that for $V_T = \Lambda$ the average enhancement computed using eq 4 for each HS is almost exactly given by the corresponding value of k_2 given in Table 1.

In summary, in this letter by making a 3D analysis of the volume trapped by regions of constant electromagnetic field enhancement and the NP surface boundary, we give a quantitative approach which provides the following:

- A new procedure to analyze the convergence of the enhancement in 3D space for arbitrary shaped NPs. This approach is more stringent than measures traditionally employed to test convergence and can readily be applied to new particles or structures that have no pre-existing well-known guidelines.
- An accurate estimation of the degree of confinement (Λ) of the enhancement (Γ) inside a given trapped volume.
- A mathematical expression for the variation of these trapped volumes as a function of the electromagnetic field enhancement.
- A method to answer the long-standing question of how far these evanescent fields would produce a significant enhancement within a certain volume around the NP.
- An accurate assessment (within the capabilities of the electrodynamic method employed) of the mean field enhancement experienced by a finite volume element such as a molecule, a quantum dot (fluorescent semiconductor NPs), located inside a hot spot.

An important direction for further work is to address the question of how to extend the present approach to HSs produced in more complex nanostructures such as nanoparticle clusters where more significant enhancements are expected. This issue would require a careful analysis but we think that the present approach is a good starting point toward predictable electrodynamic modeling of the near field enhancement.

Acknowledgment. The authors thanks CONICET, Agencia Córdoba Ciencia, Fundación Antorchas, SECYT-UNC, and FONCYT for financial support.

Supporting Information Available: Details of our implementation of the VTV approach using DDA as well as a comparison of this approach with exact electrodynamic solutions for a prolate gold spheroid. This material is available free of charge via the Internet at http://pubs.acs.org.

References and Notes

(1) Willets, K. A.; Van Duyne, R. P. *Annu. Rev. Phys. Chem.* **2007**, *58*, 267–297.

(2) Girard, C.; Martin, O. J. F.; Dereux, A. *Phys. Rev. Lett.* **1995**, *75*, 3098–3101.

(3) Kelly, K. L.; Coronado, E.; Zhao, L. L.; Schatz, G. C. *J. Phys. Chem. B* **2003**, *107* (3), 668–677.

(4) Novotny, L.; Stranick, S. J. *Annu. Rev. Phys. Chem.* **2006**, *57*, 303–31.

(5) Lee, S. J.; Guan, Z.; Xu, H.; Moskovits, M. *J. Phys. Chem. C* **2007**, *111* (49), 17985–17988.

(6) Maier, S. A. *Opt. Express* **2006**, *14* (5), 1957–1964.

(7) Stiles, P. L.; Dieringer, J. A.; Shah, N. C.; Van Duyne, R. P. *Annu. Rev. Anal. Chem.* **2008**, *1*, 601–26.

(8) Le, F.; Brandl, D. W.; Urzhumov, Y. A.; Wang, H.; Kundu, J.; Naomi J. Halas, J. A.; Nordlander, P. *ACS Nano* **2008**, *2* (4), 707–718.

(9) Bian, R. X.; Dunn, R. C.; Xie, X. S. *Phys. Rev. Lett.* **1995**, *75*, 4772–4775.

(10) Haynes, C. L.; Van Duyne, R. P. *J. Phys. Chem. B* **2003**, *107*, 7426–7433.

(11) Dieringer, J. A.; McFarland, A. D.; Shah, N. C.; Stuart, D. A.; Whitney, A. V.; Yonzon, C. R.; Young, M. A.; Zhang, X.; Van Duyne, R. P. *Faraday Discuss.* **2006**, *132*, 9–26.

(12) Zhang, W.; Cui, X.; Yeo, B.-S.; Schmid, T.; Hafner, C.; Zenobi, R. *Nano Lett.* **2008**, *7* (5), 1401–1405.

(13) Becker, M.; Sivakov, V.; Andrä, G.; Geiger, R.; Schreiber, J.; Hoffmann, S.; Michler, J.; Milenin, A. P.; Werner, P.; Christiansen, S. H. *Nano Lett.* **2007**, *7* (1), 75–80.

(14) Pettinger, B. *Top. Appl. Phys.* **2006**, *103*, 217.

(15) Stranik, O.; Nooney, R.; McDonagh, C.; MacCraith, B. D. *Plasmonics* **2007**, *2*, 15–22.

(16) Chowdhury, M. H.; Ray, K.; Aslan, K.; Lakowicz, J. R.; Geddes, C. D. *J. Phys. Chem. C* **2007**, *111*, 18856–18863.

(17) Nie, S.; Emory, S. R. *Science* **1997**, *275*, 1102–1106.

(18) Kneipp, K.; Wang, Y.; Kneipp, H.; Perelman, L. T.; Itzkan, I.; Dasari, R. R.; Feld, M. S. *Phys. Rev. Lett.* **1997**, *78*, 1667–1670.

(19) De Angelis, F.; Patrini, M.; Das, G.; Maksymov, I.; Galli, M.; Businaro, L.; Andreani, L. C.; Fabrizio, E. D. *Nano Lett.* **2008**, *8* (8), 2321–2327.

(20) Anker, J. N.; Hall, W. P.; Lyandres, O.; Shah, N. C.; Zhao, J.; Van Duyne, R. P. *Nat. Mater.* **2008**, *7*, 442–453.

(21) Srituravanich, W.; Fang, N.; Sun, C.; Luo, Q.; Zhang, X. *Nano Lett.* **2004**, *4* (6), 1085–1088.

(22) Frey, H. G.; Witt, S.; Felderer, K.; Guckenberger, R. *Phys. Rev. Lett.* **2004**, *93*, 200801.

(23) Bek, A.; Jansen, R.; Ringler, M.; Mayilo, S.; Klar, T. A.; Feldmann, J. *Nano Lett.* **2008**, *8* (2), 485–490.

(24) Tam, F.; Goodrich, G. P.; Johnson, B. R.; Halas, N. J. *Nano Lett.* **2007**, *7* (2), 496–501.

(25) Dieringer, J. A.; Wustholz, K. L.; Masiello, D. J.; Camden, J. P.; Kleinman, S. L.; Schatz, G. C.; Duyne, R. P. V. *J. Am. Chem. Soc.* **2009**, *131* (2), 849–854.

(26) Micic, M.; Klymyshyn, N.; Suh, Y. D.; Lu, H. P. *J. Phys. Chem. B* **2003**, *107*, 1574–1584.

(27) Moreno, E.; Erni, D.; Hafner, C.; Vahldieck, R. *JOSA A* **2002**, *19* (1), 101–111.

(28) Schatz, G. C.; Young, M. A.; Van Duyne, R. P. Electromagnetic Mechanism of SERS. In *Surface-Enhanced Raman Scattering -Physics and Applications*; Kneipp, K., Moskovits, M., Kneipp, H., Eds.; Springer: New York, 2006; Vol. 103, pp 19−46.

(29) Barchiesi, D.; Guizal, B.; Grosges, T. *Appl. Phys. B: Laser Opt.* **2006**, *84* (1−2), 55–60.

(30) Draine, B. T.; Flatau, P. J. *JOSA A* **2002**, *11* (4), 1491–1499.

(31) Encina, E. R.; Coronado, E. A. *J. Phys. Chem. C* **2007**, *111* (45), 16796–16801.

(32) Encina, E. R.; Coronado, E. A. *J. Phys. Chem. C* **2008**, *112* (26), 9586–9594.

(33) Coronado, E. A.; Schatz, G. C. *J. Chem. Phys.* **2003**, *119*, 3926.

(34) Hao, E.; Schatz, G. C. *J. Chem. Phys.* **2004**, *120*, 357.

(35) Palik, E. D. *Handbook of Optical Constant of Solids*; Academic Press: New York, 1985.

(36) Calandera, N.; Willander, M. *J. Appl. Phys.* **2002**, *92* (9), 4878–4884.

JP811256E